Superlattices and Microstructures 112 (2017) 561–573

Contents lists available at ScienceDirect

Superlattices and Microstructures

journal homepage: www.elsevier.com/locate/superlattices

Energy minibands degeneration induced by magnetic field effects in graphene superlattices

R.A. Reyes-Villagrana, V.H. Carrera-Escobedo, J.R. Suárez-López, J. Madrigal-Melchor, I. Rodríguez-Vargas*

Unidad Académica de Física, Universidad Autónoma de Zacatecas, Calzada Solidaridad Esquina Paseo a La Bufa S/n, Zacatecas, Zac., 98060, Mexico

ARTICLE INFO

Article history:
Received 19 July 2017
Received in revised form 13 October 2017
Accepted 14 October 2017
Available online 25 October 2017

Keywords:
Graphene superlattices
Energy minibands
Magnetic field effects

ABSTRACT

Energy minibands are a basic feature of practically any superlattice. In this regard graphene superlattices are not the exception and recently miniband transport has been reported through magneto-transport measurements. In this work, we compute the energy miniband and transport characteristics for graphene superlattices in which the energy barriers are generated by magnetic and electric fields. The transfer matrix approach and the Landauer-Büttiker formalism have been implemented to calculate the energy minibands and the linear-regime conductance. We find that energy minibands are very sensitive to the magnetic field and become degenerate by rising it. We were also able to correlate the evolution of the energy minibands as a function of the magnetic field with the transport characteristics, finding that miniband transport can be destroyed by magnetic field effects. Here, it is important to remark that although magnetic field effects have been a key element to unveil miniband transport, they can also destroy it.

1. Introduction

Graphene superlattice (GSL) is a term coined to refer to a graphene sheet subjected to a periodic modulation irrespective of the mechanism or external effect used to create the periodic pattern. The electronic and transport properties of GSLs are radically different to the corresponding ones in conventional semiconductor superlattices, thanks to the chiral nature of charge carries in graphene [1,2]. Among the most remarkable properties of GSLs we can find: highly anisotropic propagation of charge carriers [1,3–5], extra Dirac points at the Brillouin zone boundary [2–4,6–10], cloning of Dirac fermions [11], and a zero-averaged wave-number gap [12,13]. In fact, most of these novel characteristics have been confirmed experimentally [5,9–11].

Within this context, it is important to remark that one of the most relevant and general characteristic of practically any superlattice, irrespective of the elemental excitation that we are dealing with, are the so-called minibands. For instance, in conventional semiconductor superlattices energy minibands are a key factor in phenomena like negative differential conductance, Wannier-Stark localization, Bloch oscillations, resonant tunneling and electric field domains [14]. Specifically,

* Corresponding author.
E-mail address: isaac@fisica.uaz.edu.mx (I. Rodríguez-Vargas).

https://doi.org/10.1016/j.spmi.2017.10.014
0749-6036/

the width of energy minibands plays a fundamental role to understand the mentioned phenomena [14]. In graphene, energy minibands are more intricate due to the strong dependence of the electronic and transmission properties on the transversal wave vector of electrons. Moreover, energy minibands and particularly its width, are greatly influenced by the kind of external effects (barriers) that were used to generate the periodic modulation. From the experimental standpoint, energy minibands have been proven by different measurement techniques [9,15–19] that take advantage of the special features of the electronic structure, Hofstadter butterfly, that arise under the influence of a quantizing magnetic field [20]. Recently, a step forward has been given with the experimental demonstration of miniband transport in graphene [21]. In fact, this fundamental transport phenomenon was demonstrated by implementing the so-called transverse electron focusing (TEF) effect in graphene moiré superlattices. Here, it is important to stress that a magnetic field plays a central role in TEF, to such an extent that by adjusting it, ballistic miniband conduction takes place between the emitter and collector of the graphene device. Likewise, to understand, interpret and at the end to unveil miniband transport, it is quite important to know in detail the characteristics of miniband formation. In this regard, electrostatic, substrate, magnetic and strain graphene superlattices are not the exception. So, a thorough analysis of miniband formation and more importantly a detailed study of how minibands determine the transport characteristics of these superlattices is needed. In fact, some work has been done in this regard [22]. Specifically, in the case of electrostatic and substrate GSLs it was shown that the start-end, degeneration and closure of minibands determine the most important characteristics of the linear-regime conductance [22]. Under this context and taking into account the relevance of the magnetic field is that we consider that a detailed study of miniband formation and its impact on the transport properties of the so-called magnetic GSLs is necessary.

In this work, we study the electronic structure and transport properties of magnetoelectric graphene superlattices. The transfer matrix approach and the Landauer-Büttiker formalism have been implemented to obtain the energy minibands and the linear-regime conductance, respectively. We pay special attention to the effect of the magnetic field on the energy minibands as well as how this effect impacts on the transport properties. Our findings indicate that the energy minibands are pretty sensitive to the magnetic field, particularly they become degenerate by increasing it. Furthermore, we can correlate the changes in the minibands with the modifications in the conductance caused by the magnetic field. Then, it is important to keep in mind that when dealing with magnetoelectric graphene superlattices magnetic field effects can disrupt and even destroy the energy miniband characteristics, hence complicating its possible detection via transport measurements.

2. Model

The system of interest is a graphene superlattice in which the barriers are generated by magnetic and electric fields. In principle, this system can be obtained by placing ferromagnetic electrodes upon a graphene sheet in a periodic fashion, see Fig. 1a. The graphene sheet is typically deposited on a non-interacting substrate like SiO_2 with the aim that the gapless linear dispersion relation of graphene be preserved in the free regions, regions without a magnetoelectric field. This substrate together with a back gate also helps to control the Fermi energy of Dirac electrons. Here, it is also important to mention that the top ferromagnetic electrodes control the shape and distribution of the magnetic and electric fields along the superlattice

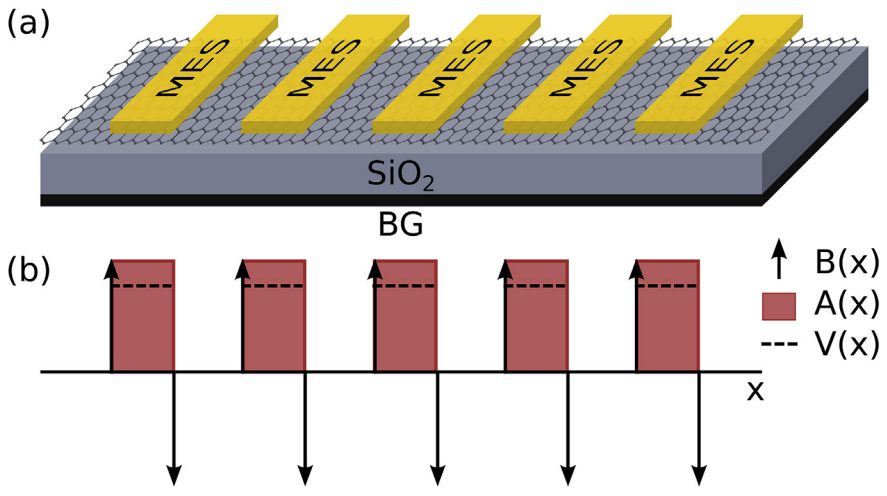

Fig. 1. (a) Schematic diagram of the possible device for magnetoelectric graphene superlattices. A typical device configuration consists of a graphene sheet deposited on a non-interacting substrate like SiO_2 (gray slab) which is usually doped, a bottom gate that controls the Fermi energy of the incident electrons, top magnetoelectric strips (MESs) that modulate the distribution and shape of the applied magnetic and electric fields, and not shown but part of the device left and right leads. (b) Distribution of the magnetic field and electrostatic potential along the superlattice axis. The magnetic field is of delta-function type, while the electrostatic potential comes in a step-wise fashion. The vector potential is also shown, it has a step-wise form as well.

axis. In our particular case, we will deal with delta-function barriers for the magnetic field and step-wise barriers for the electric field, see Fig. 1b.

To implement the transfer matrix method and consequently to obtain the transmission, transport and electronic structure properties we need the dispersion relation, wave functions and wave vectors of the barrier and well regions. Thereby, we will present in first place those quantities, afterwards, we will proceed with the basics of the transfer matrix approach, the generals of the transport formalism and the fundamentals of the electronic structure.

In the barrier regions electrons can be described by the following Dirac-like equation,

$$[v_F \sigma \cdot (\mathbf{p} + e\mathbf{A}) + V(x)\sigma_0]\psi = E\psi, \tag{1}$$

where $v_F = c/300$ is the Fermi velocity of the Dirac electrons in graphene, $\sigma = (\sigma_x, \sigma_y)$ is the vector of Pauli matrices, $\mathbf{p} = (p_x, p_y)$ is the momentum vector of electrons, $\mathbf{A} = (0, A_y, 0)$ is the vector potential, and σ_0 is the 2×2 unitary matrix. Equation (1) can be solved easily giving the dispersion relation,

$$E = U_0 \pm \sqrt{\hbar^2 v_F^2 q_x^2 + v_F^2 \left(\hbar q_y + eA_y\right)^2}, \tag{2}$$

where U_0 is the electrostatic field strength, A_y is the y component of the vector potential, q represents the two-dimensional wavevector, and the "±" signs correspond to electrons and holes, respectively. The corresponding wavefunctions, normalized to the graphene sheet area, can be written as,

$$\psi_{\pm}(x, y) = \frac{1}{\sqrt{2}} \begin{pmatrix} 1 \\ v_{\pm} \end{pmatrix} e^{\pm i q_x x + i q_y y}, \tag{3}$$

where

$$v_{\pm} = \frac{\hbar v_F \left(\pm q_x + i\left(q_y + \frac{e}{\hbar} A_y\right)\right)}{E - U_0}. \tag{4}$$

In the regions without magneto-electrostatic fields or well regions we have the usual dispersion relation,

$$E_{\pm} = \pm \hbar v_F \sqrt{k_x^2 + k_y^2}, \tag{5}$$

and wavefunctions,

$$\psi_{\pm}(x, y) = \frac{1}{\sqrt{2}} \begin{pmatrix} 1 \\ u_{\pm} \end{pmatrix} e^{\pm i k_x x + i k_y y}, \tag{6}$$

with

$$u_{\pm} = \frac{\hbar v_F (\pm k_x + i k_y)}{E}. \tag{7}$$

This information is enough to compute the transfer matrix of the system because we have $\frac{N}{2} + 1$ identical barriers and $\frac{N}{2} - 1$ identical wells. Moreover, this multi-barrier structure is enclosed by left and right semi-infinite regions with the same characteristics that well regions. Then, by taking into account the conservation of the transversal momentum, $k_y = q_y$, and imposing the continuity condition to the wavefunction in the different interfaces along the longitudinal direction (x coordinate), we can obtain a relation between the coefficients of the forward and backward wavefunction of the left semi-infinite region (A_0 and B_0) and the forward wavefunction of the right semi-infinite region (A_{N+1} and $B_{N+1} = 0$), through the transfer matrix as [23],

$$\begin{pmatrix} A_0 \\ B_0 \end{pmatrix} = M \begin{pmatrix} A_{N+1} \\ 0 \end{pmatrix}, \tag{8}$$

where the transfer matrix M is given by,

$$M = D_0^{-1} \left(\prod_{j=1}^{N} D_j P_j D_j^{-1} \right) D_t, \tag{9}$$

which is defined in terms of the dynamic D_j and propagation P_j matrices,

$$D_j = \begin{pmatrix} 1 & 1 \\ v_{+,j} & v_{-,j} \end{pmatrix}, \tag{10}$$

and

$$P_j = \begin{pmatrix} e^{-iq_{x,j}d_j} & 0 \\ 0 & e^{iq_{x,j}d_j} \end{pmatrix}, \tag{11}$$

here j = 1, 2, 3, …, N. Where D_0 and D_t are the dynamic matrix of the semi-infinite left and right regions, which in our model are the same, $D_0 = D_t$. Likewise, $q_{x,1} = q_{x,3} = q_{x,5} = \ldots = q_x$ is the x-component of the wave vector of the barriers, and $k_{x,2} = k_{x,4} = k_{x,6} = \ldots = k_x$ corresponds to the longitudinal component of the wave vector of the inter-well and semi-infinite regions. According to the characteristics of the system turns out that $v_{\pm,1} = v_{\pm,3} = v_{\pm,5} = \ldots = v_{\pm}$, $u_{\pm,2} = u_{\pm,4} = v_{\pm,6} = \ldots = u_{\pm}$ as well as $D_0 = D_2 = D_4 = \ldots = D_{N+1}$ and $D_1 = D_3 = D_5 = \ldots = D_N$. Here, D_0 and D_{N+1} correspond to the dynamic matrices of the left and right semi-infinite regions. With the transfer matrix at hand, we can calculate readily the transmission probability or transmittance,

$$T = \left|\frac{A_{N+1}}{A_0}\right| = \frac{1}{|M_{11}|^2}, \tag{12}$$

with M_{11} the $(1,1)$ element of the transfer matrix M. The linear-regime conductance is obtained through the Landauer-Bütiker formula [24],

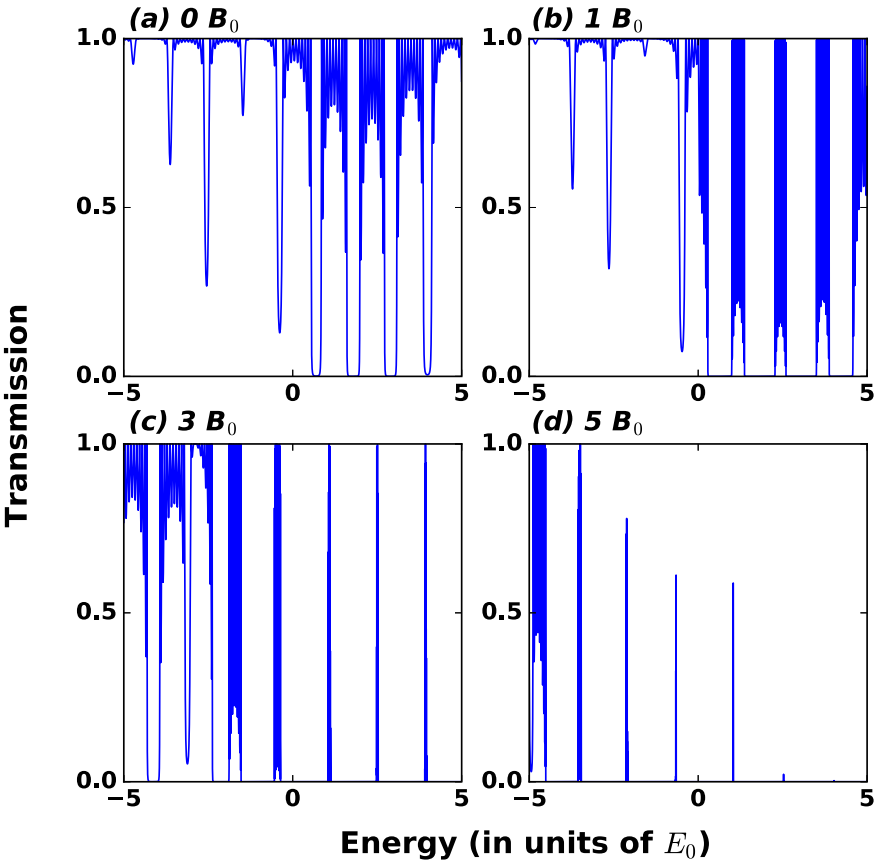

Fig. 2. Transmission probability versus the energy of incident electrons for GSLs under different magnetic field strengths: (a) $0B_0$, (b) $1B_0$, (c) $3B_0$ and (d) $5B_0$. In this case the angle of incidence, the number of periods (barriers), the widths of barriers and wells, and the height of the electrostatic barriers were $\theta = 15°$, $NP = 11$, $d_B = l_B$ and $d_w = l_B$, and $U_0 = 2E_0$, respectively.

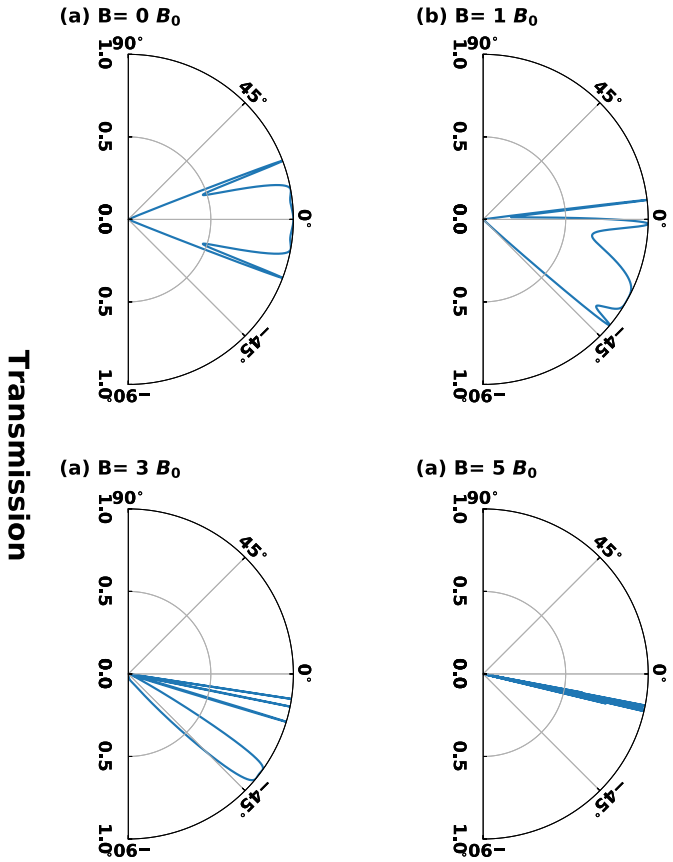

Fig. 3. Angular distribution of the transmittance of GSLs for different magnetic field strengths: (a) $0B_0$, (b) $1B_0$, (c) $3B_0$ and (d) $5B_0$. The energy considered for the impinging electrons is $E_i = 1.5E_0$. The other superlattice parameters are: $NP = 7$, $d_B = d_w = l_B$ and $U_0 = 2E_0$.

$$G/G_0 = E_F^* \int_{-\pi/2}^{\pi/2} T\left(E_F^*, \theta\right) \cos\theta d\theta, \tag{13}$$

where $E_F^* = E_F/E_0$ is the dimensionless Fermi energy with E_0 the energy unit, $G_0 = 2e^2 L_y E_0/h^2 v_F$ is the fundamental conductance factor with L_y the width of the system in the transversal y-coordinate, and θ is the angle of the incident electrons with respect to the x-coordinate. Finally, the spectrum of bound states is calculated changing from open boundary conditions to hard-wall boundary conditions, this is, the widths of the first and last barrier of the multiple structure are extended to infinity. Likewise, we have to require a pure imaginary wave vector for the semi-infinite barrier regions, which turns out in a transcendental equation between energy and transversal wave vector of Dirac electrons as,

$$M_{11}^{BS}(E, k_y; q_x \to i\alpha_x) = 0, \tag{14}$$

where q_x is the wave vector along x-coordinate defined through Equation (2) and M_{11}^{BS} the (1,1) matrix transfer of,

$$M^{BS} = D_1^{-1} \left(\prod_{j=2}^{N-2} D_j P_j D_j^{-1} \right) D_1. \tag{15}$$

here, the superscript *BS* has been included to differentiate Equation (15) from Equation (9) as well as to state that it correspond to the bound state case.

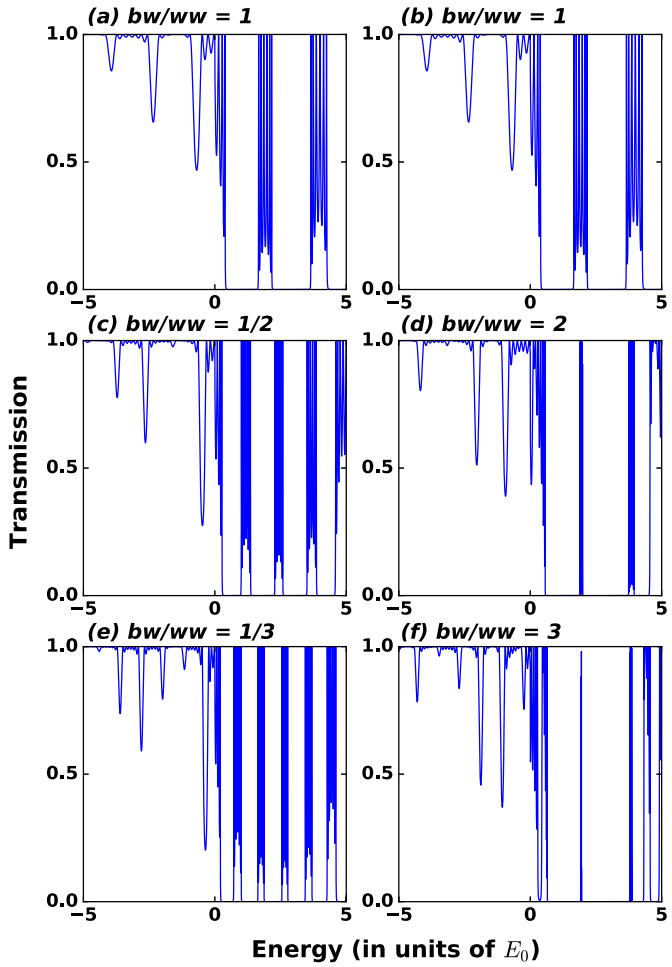

Fig. 4. Transmission probability versus the energy of incident electrons for GSLs with different width ratios of barrier to well (bw/ww): (a) and (b) $bw/ww = 1$, (c) $bw/ww = 1/2$, (d) $bw/ww = 2$, (e) $bw/ww = 1/3$ and (f) $bw/ww = 3$. Here, the magnetic field strength, the angle of incidence, the number of periods (barriers), and the height of the electrostatic barriers were $B = 1B_0$, $\theta = 15°$, $NP = 7$ and $U_0 = 2E_0$, respectively.

3. Results and discussion

Magnetic superlattices have been widely studied [25–45]. However, as far as we know there is no a systematic study of how a magnetic field modifies the energy minibands, in specific its width. Moreover, how these changes in the energy minibands are reflected in the transport properties. In a previous work [22] we have addressed the energy miniband formation and its impact on the transport properties of electrostatic superlattices. The aim of the present study is to see how a magnetic field changes the mentioned miniband formation as well as how the linear-regime conductance is affected by these changes. In order to avoid the complexities associated with an arbitrary magnetic field profile, we have considered a pretty simple deltaic magnetic field arrange in a periodic fashion in the same regions in which we have an electrostatic field, see Fig. 1b. Here, it is also important to mention that to give a complete description of the miniband characteristics we will show firstly the transmission properties, then we will proceed with the miniband structure and finally we will present the linear-regime conductance and specifically, we will try to correlate the miniband structure with the transport properties.

As it is well known the transmission properties of GSLs are pretty sensitive to the angle of incidence of the impinging electrons. So, we will focus our attention on the effect of the magnetic field strength by keeping the angle of incidence and the other parameters of the superlattice (well and barrier widths, barrier heights and number of periods) fixed. In the present study, the magnetic field strength will come in terms of a reference field $B_0 = 0.1$ T. Likewise, the lengths and the energies will be given in terms of the so-called magnetic length $l_B = \sqrt{\hbar/eB_0} = 811$ Å and its associated energy $E_0 = \hbar v_F/l_B = 7.0$ meV, respectively. The y-component of the vector potential will come in terms of the magnetic field strength as well as the magnetic length, $A_y = B(B_0)l_B$. As we are primordially interested in the magnetic field effects, the height of the electrostatic

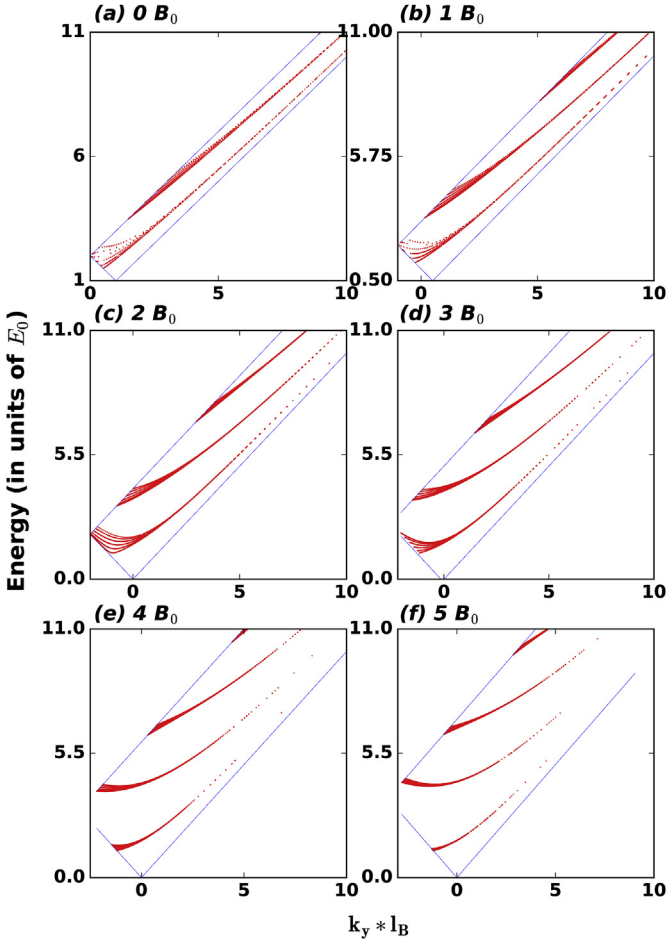

Fig. 5. Miniband structure versus k_y for GSLs under different magnetic field strengths: (a) $0B_0$, (b) $1B_0$, (c) $2B_0$, (d) $3B_0$, (e) $4B_0$ and (f) $5B_0$. In this case the number of periods (barriers), the widths of barriers and wells, and the height of the electrostatic barriers were $NP = 7$, $d_B = l_B$ and $d_w = l_B$, and $U_0 = 2E_0$, respectively. The solid-blue lines divide the regions of bound and propagating states. (For interpretation of the references to colour in this figure legend, the reader is referred to the web version of this article.)

barriers will be the same throughout the study. In specific, we will work with $U_0 = 2E_0$. At this point, it is important to mention that we need to consider oblique incidence ($\theta = 15^\circ$) because otherwise there is no miniband formation due to the so-called Klein tunneling. In Fig. 2 we show how energy minibands evolve as the magnetic filed increases. The case of $B = 0$ T corresponds to a pure electrostatic superlattice, and consequently, we can see well-defined minibands in which the number of resonances within them correspond to the number of superlattice periods. Once the magnetic field is incorporated the width of minibands is reduced and the resonances within the minibands tend to overlap. Even more, if the magnetic field is strong enough, the minibands collapse and become a simple resonance, in other words, minibands degenerate as the magnetic field rises. We also want to remark that the angle of incidence should guarantee miniband structure. Even more, if we are interested in analyzing the evolution of minibands as a function of the magnetic field. Regarding this, it is well known that in electrostatic GSLs minibands collapse if the angle of incidence is large [46]. This can be even more dramatic if we consider magnetic field effects. For instance, the angular distribution of the transmittance is quite sensitive to the magnetic field, see Fig. 3. Actually, once the magnetic field is incorporated the angular distribution is no longer symmetric. Furthermore, for large magnetic fields the transmittance is reduced to a very narrow angular range, see Fig. 3d. Under this context, $\theta = 15^\circ$ in Fig. 2 is not a special angle, but it is an angle that allows us to analyze the evolution of minibands for different magnetic field strengths.

Another parameter that can be quite useful to control the number of minibands, as well as the width of them within an energy range, is the ratio between widths of the barrier and well, bw/ww. In Fig. 4 we show our results for ratios less than one and greater than one, first and second column of the panel, respectively. As we can see for $bw/ww < 1$, that is, for well widths greater then the barrier widths, the number of minibands is increased as the ratio is reduced. For instance, when $bw/ww = 1$ the number of well-formed minibands is two, but for $bw/ww = 1/2$ this number increases to four and for $bw/ww = 1/3$ the number becomes five. On the contrary, when $bw/ww > 1$ the already established minibands for $bw/ww = 1$ diminish in its

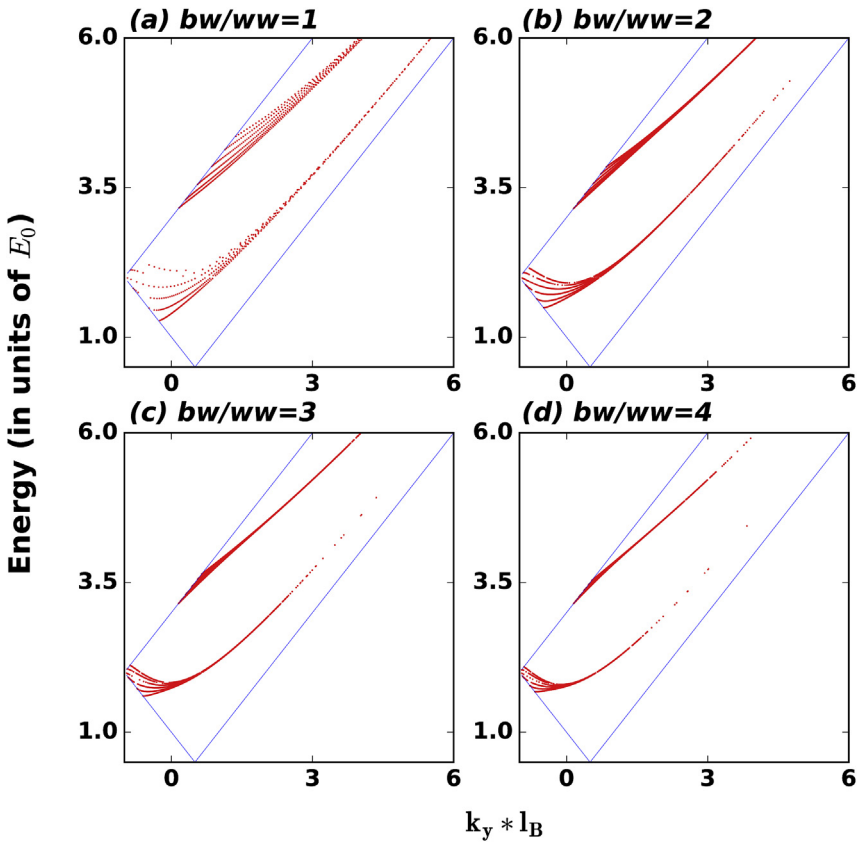

Fig. 6. Miniband structure versus k_y for GSLs with different width ratios of barrier to well: (a) $bw/ww = 1$, (b) $bw/ww = 2$, (c) $bw/ww = 3$ and (d) $bw/ww = 4$. Here, the magnetic field strength, the number of periods (barriers), and the height of the electrostatic barriers were $B = 1B_0$, $NP = 7$ and $U_0 = 2E_0$, respectively. The solid-blue lines divide the regions of bound and propagating states. (For interpretation of the references to colour in this figure legend, the reader is referred to the web version of this article.)

width and eventually tend to collapse to very narrow minibands, even to a single resonance. This latter case is equivalent to the effect caused by the magnetic field. These results are quite relevant because the current experimental techniques allow to discriminate the transport properties at angular level [47–50]. Then, if we want to observe miniband transport it is very important to choose appropriately the structural parameters of the superlattice as well as the strength of the applied magnetic field.

As we previously pointed out the computation of the miniband structure is fundamental to understand the features of the conductance curves. Thereby, we will show the energy level structure as a function of the transversal wave vector for different magnetic field strengths, Fig. 5. In fact, when there is no magnetic field applied to the system we can see the typical energy level structures for electrostatic superlattices, that is, we have minibands that depend strongly on the transversal wave vector. Particularly, minbands have a well-defined width for small transversal wave vectors and they become degenerate for large wave vectors. Once the magnetic field is considered, at first instance, the relevant region for the computation of bound states is modified. Specifically, this region is bigger and spans to negative wave vectors [51]. At second instance, the number of minibands increases as the magnetic field rises. And third instance, and more importantly, the width of minibands at small wave vectors diminishes as the strength of the magnetic field increases. In fact, minibands can degenerate at a critical magnetic field in staircase fashion, that is, the first, second and third minibands will degenerate consecutively as the magnetic field rises. A similar effect can be achieved with the ratio between the width of the barrier and well, while keeping the magnetic field fixed, see Fig. 6.

Now it is turn to analyze the conductance as a function of the Fermi energy for different magnetic field strengths. We have considered the same magnetic fields as in the case of the miniband structure, namely: 0, 1, 2, 3, 4 and 5 in units of B_0, Fig. 7a, b, c, d, e and f, respectively. For $B = 0$ we can see the well known oscillating behavior of the conductance for electrostatic GSLs. Here, it is important to remark that the conductance peaks are smooth and with practically no internal structure. Once the magnetic field is incorporated the conductance peaks present internal structure. In concrete, each peak has a series of small peaks (oscillations) that in number correspond to the number of wells in the superlattice. Another important feature of the conductance curves under magnetic field effects is that its line-shape resembles the one of substrate-based GSLs [22]. This result is quite interesting because the magnetic field effects and the substrate-based effects are not at all equivalent. It is also

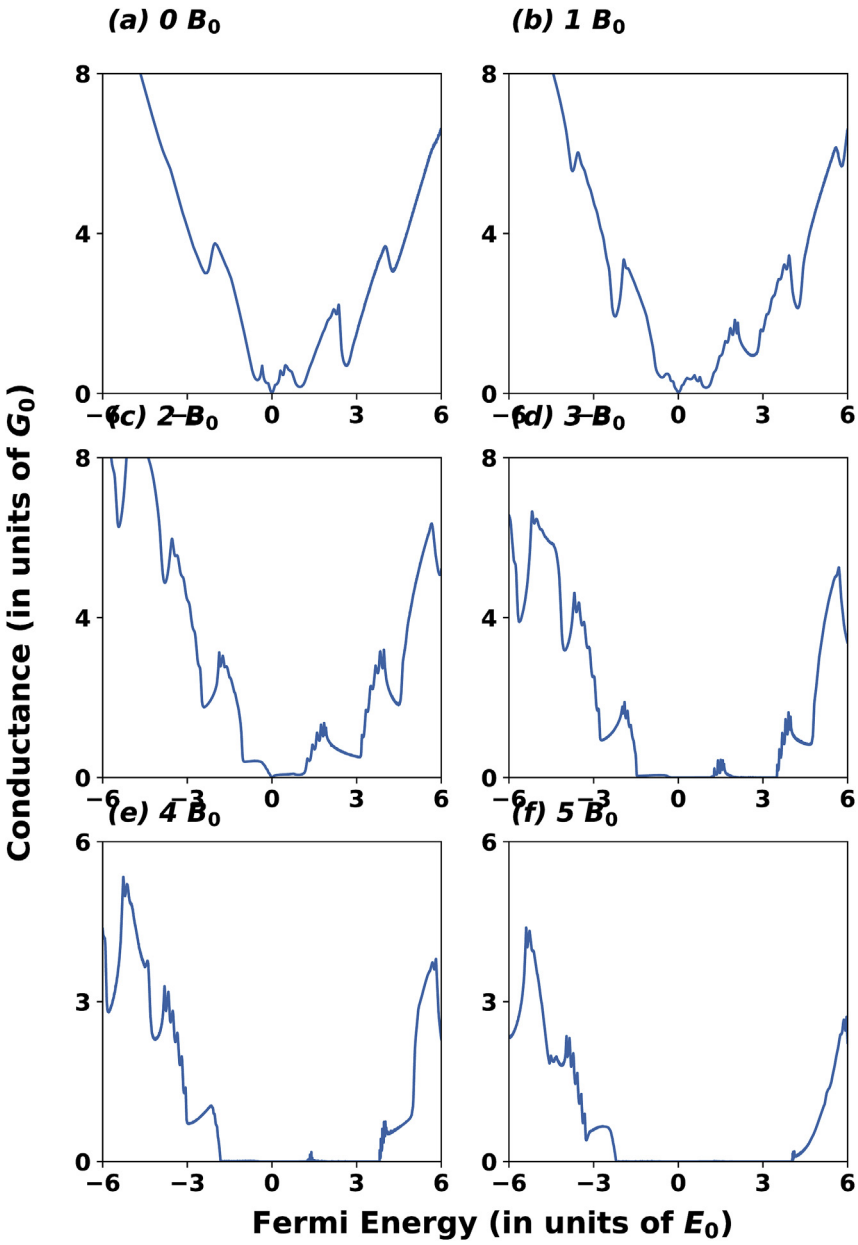

Fig. 7. Conductance versus Fermi energy for GSLs under different magnetic field strengths: (a) $0B_0$, (b) $1B_0$, (c) $2B_0$, (d) $3B_0$, (e) $4B_0$ and (f) $5B_0$. In this case, the number of periods (barriers), the widths of barriers and wells, and the height of the electrostatic barriers were $NP = 7$, $d_B = l_B$ and $d_w = l_B$, and $U_0 = 2E_0$, respectively.

worth mentioning that the small oscillations are direct evidence of miniband transport. In this sense, the magnetic field effects are welcomed because they unveil the characteristics of minibands directly on the transport properties. Aspect that is not at all reachable in electrostatic GSLs. Unfortunately, not all is good with the magnetic field because for large magnetic field strengths the characteristics of miniband transport tend to disappear, see Fig. 7d, e and f. Even more, if the magnetic field is large enough, a huge conductance gap is created. This gap could be important for certain applications, but certainly not for miniband transport. Similar results are achievable by changing the ratio between the widths of barriers and wells, see Fig. 8. Therefore, to get the characteristics of miniband transport it is quite important to take care of the fundamental parameters of the superlattice as well as the strength of the applied magnetic field.

Another aspect that we want to address is the connection that we can be established between the miniband structure and the transport properties. In particular, the onset and end of the minibands at small wave vectors determine the main features

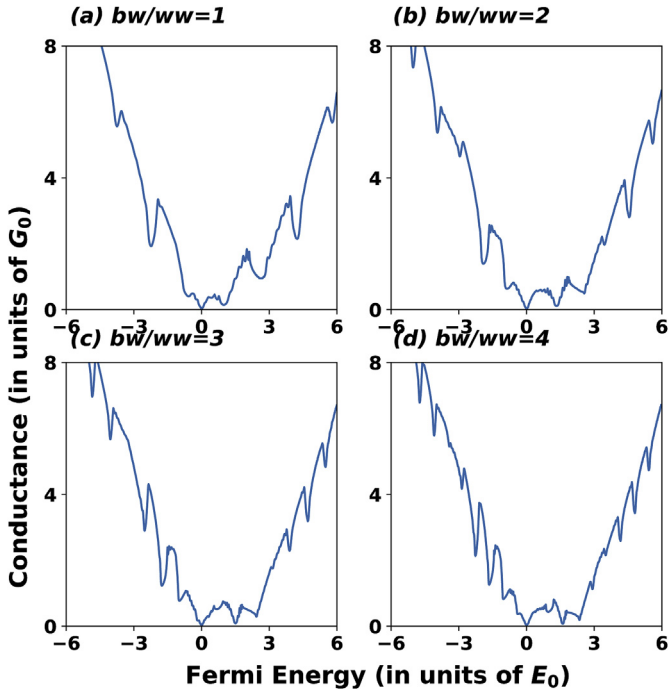

Fig. 8. Conductance versus Fermi energy for GSLs with different width ratios of barrier to well: (a) $bw/ww = 1$, (b) $bw/ww = 2$, (c) $bw/ww = 3$ and (d) $bw/ww = 4$. Here, the magnetic field strength, the number of periods (barriers), and the height of the electrostatic barriers were $B = 1B_0$, $NP = 7$ and $U_0 = 2E_0$, respectively.

of the peaks of the conductance curves [22]. For instance, the oscillations in each conductance peak start at the onset of the minibands and the sudden slump that defines the line-shape of the conductance peaks coincides with the end of the minibands. The miniband degeneration, the collapsing of minibands into a practically a single subband, also plays an important role, since the minimums and the sudden rise of the conductance are taking place at energy regions in which the degeneration is presented. Furthermore, the small peaks that define the oscillations within each main conductance peak agree quite well with the location of the subband levels at small wave vectors within each miniband. All these characteristics can be destroyed if the magnetic field is large and/or if the ratio of the width of the barrier to well is large as well. In Fig. 9 we show in the same graphs the miniband structure and the conductance in order to illustrate the matching between the energy level structure and the main characteristics of the transport properties as mentioned.

Finally, we would like to explain as far as possible the origin of the degeneration of minibands under magnetic field effects. In order to do that, we will consider the fundamental aspect that gives place to the formation of minibands, which is the overlapping of wave functions between neighboring quantum wells. In fact, it is well known that if the overlapping between wave functions is negligible there is no splitting between energy levels and consequently there is no formation of energy minibands. In conventional semiconductor superlattices, the parameters, that in great extent, mediate the mentioned overlapping are the width and height of the barriers. In GSLs we have two additional factors that can affect greatly the wave function overlapping, one is the transversal wave vector k_y and the other is the applied magnetic field. These parameters enter directly in the barrier wave vector $\hbar v_F q_x = \sqrt{(E - V_0)^2 - v_F(\hbar q_y + eA_y)^2}$. Hence, when the magnetic field is increased the electronic structure of GSLs is greatly modified, particularly the overlapping of the wave functions diminishes. For instance, if the term of the magnetic field, for fixed transversal wave vector, dominates over the term $(E - V_0)^2$ the wave functions become evanescent and their penetration into the barriers, if the magnetic field is strong, will be practically negligible, consequently there will be no room to formation of energy minibands. Likewise, if the magnetic field dominates there will be no room for propagation, and consequently a conductance gap will arise. This gap will increase as the magnetic field rises. Lastly, as we have testified the fundamental properties of GSLs can be modified readily through magnetic field effects. So, these effects can be useful in possible technological applications such as electronic filters, transistors, diodes and laser based on GSLs.

4. Conclusions

In summary, we study the electronic and transport properties of magnetoelectric graphene superlattices. The transfer matrix approach and the Landauer-Büttiker formalism have been implemented to obtain the energy minibands structure and the linear-regime conductance, respectively. We have paid special attention to the effects of the magnetic field on the energy

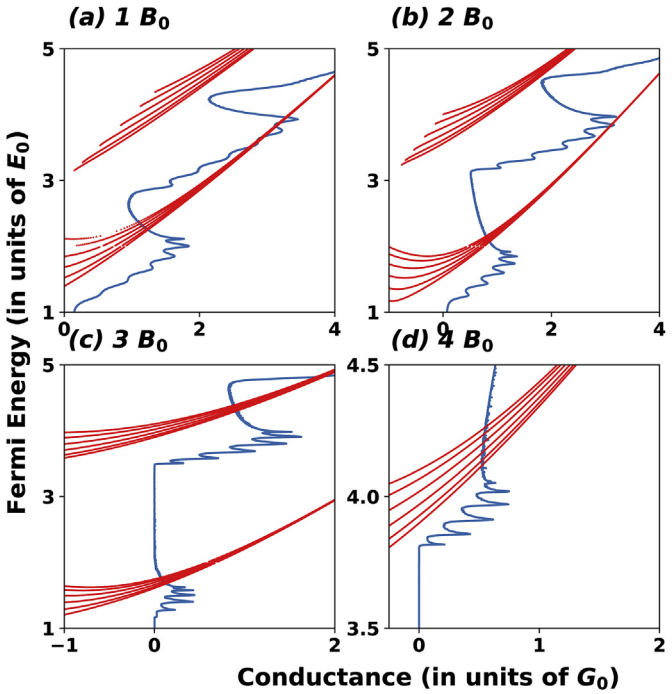

Fig. 9. Correspondence of the conductance characteristics (blue curves) with the miniband structure (red lines) for GSLs under different magnetic field strengths: (a) $1B_0$, (b) $2B_0$, (c) $3B_0$ and (d) $4B_0$. As we can notice the width of the main conductance peaks corresponds to the effective width of minibands at small wave vectors and the oscillations (small peaks) within each mean peak correspond to subbands within each miniband. The basic parameters of the superlattice were $NP = 7$, $d_B = d_w = l_B$ and $U_0 = 2E_0$. (For interpretation of the references to colour in this figure legend, the reader is referred to the web version of this article.)

minibands as well as how these effects change the transport characteristics. Our findings indicate that the already intricate energy minibands structure of GSLs is greatly affected by the magnetic field. Particularly, energy minibands become degenerate as the magnetic field is increased. In the case of the linear-regime conductance we were able to identify the energy and wave vector regions in which miniband transport is taking place. We also find that the magnetic field can disrupt, modify and even destroy those characteristics associated with miniband transport.

Acknowledgements

The author R. A. Reyes-Villagrana acknowledge the support of post-doctoral residence of PRODEP.

References

[1] C.-H. Park, L. Yang, Y.-W. Son, M.L. Cohen, S.G. Louie, Anisotropic behaviours of massless dirac fermions in graphene under periodic potentials, Nat. Phys. 4 (3) (2008) 213–217, https://doi.org/10.1038/nphys890.
[2] C.-H. Park, L. Yang, Y.-W. Son, M.L. Cohen, S.G. Louie, New generation of massless dirac fermions in graphene under external periodic potentials, Phys. Rev. Lett. 101 (2008) 126804, https://doi.org/10.1103/PhysRevLett.101.126804.
[3] P. Burset, A.L. Yeyati, L. Brey, H.A. Fertig, Transport in superlattices on single-layer graphene, Phys. Rev. B 83 (2011) 195434, https://doi.org/10.1103/PhysRevB.83.195434.
[4] L. Dell'Anna, A. De Martino, Magnetic superlattice and finite-energy dirac points in graphene, Phys. Rev. B 83 (2011) 155449, https://doi.org/10.1103/PhysRevB.83.155449.
[5] S. Rusponi, M. Papagno, P. Moras, S. Vlaic, M. Etzkorn, P.M. Sheverdyaeva, D. Pacilé, H. Brune, C. Carbone, Highly anisotropic dirac cones in epitaxial graphene modulated by an island superlattice, Phys. Rev. Lett. 105 (2010) 246803, https://doi.org/10.1103/PhysRevLett.105.246803.
[6] M. Barbier, P. Vasilopoulos, F.M. Peeters, Extra dirac points in the energy spectrum for superlattices on single-layer graphene, Phys. Rev. B 81 (2010) 075438, https://doi.org/10.1103/PhysRevB.81.075438.
[7] X.-X. Guo, D. Liu, Y.-X. Li, Conductance and shot noise in graphene superlattice, Appl. Phys. Lett. 98 (24) (2011) 242101, https://doi.org/10.1063/1.3599447.
[8] G.M. Maksimova, E.S. Azarova, A.V. Telezhnikov, V.A. Burdov, Graphene superlattice with periodically modulated dirac gap, Phys. Rev. B 86 (2012) 205422, https://doi.org/10.1103/PhysRevB.86.205422.
[9] M. Yankowitz, J. Xue, D. Cormode, J.D. Sanchez-Yamagishi, K. Watanabe, T. Taniguchi, P. Jarillo-Herrero, P. Jacquod, B.J. LeRoy, Emergence of superlattice dirac points in graphene on hexagonal boron nitride, Nat. Phys. 8 (5) (2012) 382–386, https://doi.org/10.1038/nphys2272.
[10] H. Yan, Z.-D. Chu, W. Yan, M. Liu, L. Meng, M. Yang, Y. Fan, J. Wang, R.-F. Dou, Y. Zhang, Z. Liu, J.-C. Nie, L. He, Superlattice dirac points and space-dependent fermi velocity in a corrugated graphene monolayer, Phys. Rev. B 87 (2013) 075405, https://doi.org/10.1103/PhysRevB.87.075405.
[11] L.A. Ponomarenko, R.V. Gorbachev, G.L. Yu, D.C. Elias, R. Jalil, A.A. Patel, A. Mishchenko, A.S. Mayorov, C.R. Woods, J.R. Wallbank, M. Mucha-Kruczynski, B.A. Piot, M. Potemski, I.V. Grigorieva, K.S. Novoselov, F. Guinea, V.I. Fal'ko, A.K. Geim, Cloning of dirac fermions in graphene superlattices, Nature 497 (7451) (2013) 594–597, https://doi.org/10.1038/nature12187.

[12] L.-G. Wang, S.-Y. Zhu, Electronic band gaps and transport properties in graphene superlattices with one-dimensional periodic potentials of square barriers, Phys. Rev. B 81 (2010) 205444, https://doi.org/10.1103/PhysRevB.81.205444.
[13] L.-G. Wang, X. Chen, Robust zero-averaged wave-number gap inside gapped graphene superlattices, J. Appl. Phys. 109 (3) (2011) 033710, https://doi.org/10.1063/1.3525270.
[14] H.T. Grahn, Semiconductor Superlattices: Growth and Electronic Properties, World Scientific, 1995.
[15] W. Yang, X. Lu, G. Chen, S. Wu, G. Xie, M. Cheng, D. Wang, R. Yang, D. Shi, K. Watanabe, T. Taniguchi, C. Voisin, B. Plaçais, Y. Zhang, G. Zhang, Hofstadter butterfly and many-body effects in epitaxial graphene superlattice, Nano Lett. 16 (4) (2016) 2387–2392, https://doi.org/10.1021/acs.nanolett.5b05161 pMID: 26950258.
[16] B. Hunt, J.D. Sanchez-Yamagishi, A.F. Young, M. Yankowitz, B.J. LeRoy, K. Watanabe, T. Taniguchi, P. Moon, M. Koshino, P. Jarillo-Herrero, R.C. Ashoori, Massive dirac fermions and hofstadter butterfly in a van der waals heterostructure, Science 340 (6139) (2013) 1427–1430, https://doi.org/10.1126/science.1237240. http://science.sciencemag.org/content/340/6139/1427.full.pdf.
[17] C.R. Dean, L. Wang, P. Maher, C. Forsythe, F. Ghahari, Y. Gao, J. Katoch, M. Ishigami, P. Moon, M. Koshino, T. Taniguchi, K. Watanabe, K.L. Shepard, J. Hone, P. Kim, Hofstadter/'s butterfly and the fractal quantum hall effect in moire superlattices, Nature 497 (7451) (2013) 598–602, https://doi.org/10.1038/nature12186.
[18] L.A. Ponomarenko, R.V. Gorbachev, G.L. Yu, D.C. Elias, R. Jalil, A.A. Patel, A. Mishchenko, A.S. Mayorov, C.R. Woods, J.R. Wallbank, M. Mucha-Kruczynski, B.A. Piot, M. Potemski, I.V. Grigorieva, K.S. Novoselov, F. Guinea, V.I. Fal'ko, A.K. Geim, Cloning of dirac fermions in graphene superlattices, Nature 497 (7451) (2013) 594–597, https://doi.org/10.1038/nature12187.
[19] G.L. Yu, R.V. Gorbachev, J.S. Tu, A.V. Kretinin, Y. Cao, R. Jalil, F. Withers, L.A. Ponomarenko, B.A. Piot, M. Potemski, D.C. Elias, X. Chen, K. Watanabe, T. Taniguchi, I.V. Grigorieva, K.S. Novoselov, V.I. Fal'ko, A.K. Geim, A. Mishchenko, Hierarchy of hofstadter states and replica quantum hall ferromagnetism in graphene superlattices, Nat. Phys. 10 (7) (2014) 525–529, https://doi.org/10.1038/nphys2979.
[20] D.R. Hofstadter, Energy levels and wave functions of bloch electrons in rational and irrational magnetic fields, Phys. Rev. B 14 (1976) 2239–2249, https://doi.org/10.1103/PhysRevB.14.2239.
[21] M. Lee, J.R. Wallbank, P. Gallagher, K. Watanabe, T. Taniguchi, V.I. Fal'ko, D. Goldhaber-Gordon, Ballistic miniband conduction in a graphene superlattice, Science 353 (6307) (2016) 1526–1529, https://doi.org/10.1126/science.aaf1095. http://science.sciencemag.org/content/353/6307/1526.full.pdf.
[22] J. Briones-Torres, J. Madrigal-Melchor, J. Martínez-Orozco, I. Rodríguez-Vargas, Electrostatic and substrate-based monolayer graphene superlattices: energy minibands and its relation with the characteristics of the conductance curves, Superlattice. Microstruct. 73 (2014) 98–112, https://doi.org/10.1016/j.spmi.2014.05.028. http://www.sciencedirect.com/science/article/pii/S0749603614001876.
[23] P. Yeh, Optical Waves Layered Media, Wiley, 2005.
[24] S. Datta, Electronic Transport in Mesoscopic System, Cambridge University Press, 1997.
[25] M. Tahir, K. Sabeeh, Quantum transport of dirac electrons in graphene in the presence of a spatially modulated magnetic field, Phys. Rev. B 77 (2008) 195421, https://doi.org/10.1103/PhysRevB.77.195421.
[26] Q.-S. Wu, S.-N. Zhang, S.-J. Yang, Transport of the graphene electrons through a magnetic superlattice, J. Phys. Condens. Matter 20 (48) (2008) 485210. http://stacks.iop.org/0953-8984/20/i=48/a=485210.
[27] M.R. Masir, P. Vasilopoulos, F.M. Peeters, Wavevector filtering through single-layer and bilayer graphene with magnetic barrier structures, Appl. Phys. Lett. 93 (24) (2008) 242103, https://doi.org/10.1063/1.3049600.
[28] L. Dell'Anna, A. De Martino, Multiple magnetic barriers in graphene, Phys. Rev. B 79 (2009) 045420, https://doi.org/10.1103/PhysRevB.79.045420.
[29] M.R. Masir, P. Vasilopoulos, F.M. Peeters, Magnetic kronig–penney model for dirac electrons in single-layer graphene, New J. Phys. 11 (9) (2009), 095009, http://stacks.iop.org/1367-2630/11/i=9/a=095009.
[30] Y.-X. Li, Transport in a magnetic field modulated graphene superlattice, J. Phys. Condens. Matter 22 (1) (2010), 015302, http://stacks.iop.org/0953-8984/22/i=1/a=015302.
[31] R. Nasir, K. Sabeeh, M. Tahir, Magnetotransport in a periodically modulated graphene monolayer, Phys. Rev. B 81 (2010) 085402, https://doi.org/10.1103/PhysRevB.81.085402.
[32] L.Z. Tan, C.-H. Park, S.G. Louie, Graphene dirac fermions in one-dimensional inhomogeneous field profiles: transforming magnetic to electric field, Phys. Rev. B 81 (2010) 195426, https://doi.org/10.1103/PhysRevB.81.195426.
[33] R. Biswas, A. Biswas, N. Hui, C. Sinha, Ballistic transport through electric field modulated graphene periodic magnetic barriers, J. Appl. Phys. 108 (4) (2010) 043708, https://doi.org/10.1063/1.3467778.
[34] L. Sun, C. Fang, Y. Song, Y. Guo, Transport properties through graphene-based fractal and periodic magnetic barriers, J. Phys. Condens. Matter 22 (44) (2010), 445303, http://stacks.iop.org/0953-8984/22/i=44/a=445303.
[35] J.-H. Lee, J.C. Grossman, Magnetic properties in graphene-graphane superlattices, Appl. Phys. Lett. 97 (13) (2010) 133102, https://doi.org/10.1063/1.3495771.
[36] J. Sun, H.A. Fertig, L. Brey, Effective magnetic fields in graphene superlattices, Phys. Rev. Lett. 105 (2010) 156801, https://doi.org/10.1103/PhysRevLett.105.156801.
[37] L. Dell'Anna, A. De Martino, Magnetic superlattice and finite-energy dirac points in graphene, Phys. Rev. B 83 (2011) 155449, https://doi.org/10.1103/PhysRevB.83.155449.
[38] X.-X. Guo, D. Liu, Y.-X. Li, Conductance and shot noise in graphene superlattice, Appl. Phys. Lett. 98 (24) (2011) 242101, https://doi.org/10.1063/1.3599447.
[39] Q.-R. Ke, H.-F. Lü, X.-D. Chen, X.-T. Zu, Enhanced spin polarization in an asymmetric magnetic graphene superlattice, Solid State Commun. 151 (17) (2011) 1131–1134, https://doi.org/10.1016/j.ssc.2011.05.026 http://www.sciencedirect.com/science/article/pii/S0038109811002626.
[40] L. Jiang, Y. Zheng, Magnetic miniband and magnetotransport property of a graphene superlattice, J. Appl. Phys. 109 (5) (2011) 053701, https://doi.org/10.1063/1.3553582.
[41] S.F. Islam, N.K. Singh, T.K. Ghosh, Thermodynamic properties of a magnetically modulated graphene monolayer, J. Phys. Condens. Matter 23 (44) (2011), 445502, http://stacks.iop.org/0953-8984/23/i=44/a=445502.
[42] W.-T. Lu, Y.-L. Wang, C.-Z. Ye, H. Jiang, W. Li, Resonant peak splitting through magnetic kronig–penney superlattices in graphene, Phys. B Condens. Matter 407 (24) (2012) 4735–4737, https://doi.org/10.1016/j.physb.2012.09.014. http://www.sciencedirect.com/science/article/pii/S0921452612008708.
[43] F. Sattari, E. Faizabadi, Tunneling time and hartman effect in a ferromagnetic graphene superlattice, AIP Adv. 2 (1) (2012) 012123, https://doi.org/10.1063/1.3681190.
[44] W.-T. Lu, S.-J. Wang, Y.-L. Wang, H. Jiang, W. Li, Transport properties of graphene under periodic and quasiperiodic magnetic superlattices, Phys. Lett. A 377 (19) (2013) 1368–1372, https://doi.org/10.1016/j.physleta.2013.03.035. http://www.sciencedirect.com/science/article/pii/S0375960113003204.
[45] L. Zheng-Fang, W. Qing-Ping, L. Nian-Hua, Electronic energy band and transport properties in monolayer graphene with periodically modulated magnetic vector potential and electrostatic potential, Commun. Theor. Phys. 57 (2) (2012) 315. http://stacks.iop.org/0253-6102/57/i=2/a=25.
[46] H. Garíca-Cervantes, L.M. Gaggero-Sager, O. Sotolongo-Costa, G.G. Naumis, I. Rodríguez-Vargas, Angle-dependent bandgap engineering in gated graphene superlattices, AIP Adv. 6 (3) (2016) 035309, https://doi.org/10.1063/1.4944495.
[47] A. Rahman, J.W. Guikema, N.M. Hassan, N. Marković, Angle-dependent transmission in graphene heterojunctions, Appl. Phys. Lett. 106 (1) (2015) 013112, https://doi.org/10.1063/1.4905566.
[48] R.N. Sajjad, A.W. Ghosh, Manipulating chiral transmission by gate geometry: switching in graphene with transmission gaps, ACS Nano 7 (11) (2013) 9808–9813, https://doi.org/10.1021/nn403336n.
[49] R.N. Sajjad, S. Sutar, J.U. Lee, A.W. Ghosh, Manifestation of chiral tunneling at a tilted graphene *p-n* junction, Phys. Rev. B 86 (2012) 155412, https://doi.org/10.1103/PhysRevB.86.155412.

[50] S. Sutar, E.S. Comfort, J. Liu, T. Taniguchi, K. Watanabe, J.U. Lee, Angle-dependent carrier transmission in graphene p–n junctions, Nano Lett. 12 (9) (2012) 4460–4464, https://doi.org/10.1021/nl3011897 pMID: 22873738.
[51] V. Carrera-Escobedo, J. Suárez-López, J. Martínez-Orozco, J. Madrigal-Melchor, I. Rodríguez-Vargas, Magnetoelectric barriers in monolayer graphene: red and blue shifts of the low energy conductance peaks and its relation to the spectrum of bound states, Phys. E Low-dimensional Syst. Nanostruct. 63 (2014) 248–258, https://doi.org/10.1016/j.physe.2014.06.008 http://www.sciencedirect.com/science/article/pii/S1386947714002240.